Anisotropic magnetism and spin-dependent transport in Co nanoparticle embedded ZnO thin films

D. Y. Li, Y. J. Zeng, L. M. C. Pereira, D. Batuk, J. Hadermann, Y. Z. Zhang, Z. Z. Ye, K. Temst, A. Vantomme, M. J. Van Bael, and C. Van Haesendonck

Citation: Journal of Applied Physics **114**, 033909 (2013); doi: 10.1063/1.4815877
View online: http://dx.doi.org/10.1063/1.4815877
View Table of Contents: http://scitation.aip.org/content/aip/journal/jap/114/3?ver=pdfcov
Published by the AIP Publishing

Anisotropic magnetism and spin-dependent transport in Co nanoparticle embedded ZnO thin films

D. Y. Li,[1] Y. J. Zeng,[1,a)] L. M. C. Pereira,[2] D. Batuk,[3] J. Hadermann,[3] Y. Z. Zhang,[4] Z. Z. Ye,[4] K. Temst,[2] A. Vantomme,[2] M. J. Van Bael,[1] and C. Van Haesendonck[1]
[1]*Laboratory of Solid-State Physics and Magnetism, KU Leuven, Celestijnenlaan 200 D, BE-3001 Leuven, Belgium*
[2]*Instituut voor Kern- en Stralingsfysica, KU Leuven, Celestijnenlaan 200 D, BE-3001 Leuven, Belgium*
[3]*Electron Microscopy for Materials Science – EMAT, University of Antwerp, Groenenborgerlaan 171, BE-2020 Antwerp, Belgium*
[4]*State Key Laboratory of Silicon Materials, Department of Materials Science and Engineering, Zhejiang University, Hangzhou 310027, People's Republic of China*

(Received 30 May 2013; accepted 27 June 2013; published online 17 July 2013)

Oriented Co nanoparticles were obtained by Co ion implantation in crystalline ZnO thin films grown by pulsed laser deposition. Transmission electron microscopy revealed the presence of elliptically shaped Co precipitates with nanometer size, which are embedded in the ZnO thin films, resulting in anisotropic magnetic behavior. The low-temperature resistance of the Co-implanted ZnO thin films follows the Efros-Shklovskii type variable-range-hopping. Large negative magnetoresistance (MR) exceeding 10% is observed in a magnetic field of 1 T at 2.5 K and the negative MR survives up to 250 K (0.3%). The negative MR reveals hysteresis as well as anisotropy that correlate well with the magnetic properties, clearly demonstrating the presence of spin-dependent transport. © *2013 AIP Publishing LLC*. [http://dx.doi.org/10.1063/1.4815877]

I. INTRODUCTION

Magnetic semiconductors (MSs) and related hybrid systems have attracted intensive research interest in recent years due to their promising applications in spintronics.[1–4] At the crossing between semiconductor physics, magnetism, and magnetoelectrics, MSs provide multifunctional properties for next generation devices. Granular systems are interesting candidate materials for obtaining MSs. Their spin-dependent transport has first been demonstrated in metallic systems, such as the immiscible Cu-Co system,[5,6] as an alternative for the multilayer giant magnetoresistance (GMR) system. Consequently, it appears appealing to extend this research to granular ferromagnetic grains embedded in a semiconducting or insulating matrix, as this opens opportunities for combining spintronics with well-established semiconductor based electronics. A number of investigations have been reported so far including investigations on Ni-SiO_2,[7] Fe-Si,[8] Mn-Ge,[9] and Ni-$LaSrMnO_3$.[10] Among the possible choices granular ZnO-based MSs doped with 3d-transition metals are of particular interest due to the many excellent properties of ZnO, including piezoelectricity, optoelectronic response, as well as non-toxicity and abundance in nature.[11] Thus, finding a good magnetoelectric response may pave the way to develop ZnO-based spintronics. Various methods have been used to fabricate ZnO-based MSs, including pulsed laser deposition (PLD),[12] sputtering,[13] ion implantation,[14–16] and electrochemical deposition.[17] In terms of applications ion implantation offers a convenient way to control dopant species and concentration. In previous studies of the ZnO:Co system the magnetic properties have been investigated in detail,[18] while the magnetotransport and, in particular, the anisotropy have been less covered. Most of the reported magnetotransport properties turned out to be complicated or controversial and lacked spin-dependent signatures.[19–22]

Here, we rely on high-fluence Co implantation to obtain Co nanoparticles embedded in a ZnO matrix. Using magnetoresistance (MR) and magnetization measurements we obtain clear evidence for spin-dependent transport with anisotropic properties up to room temperature.

II. EXPERIMENTAL DETAILS

ZnO thin films with a thickness of 100 nm were grown by PLD on Si/SiO_2 substrates with a top layer of 300 nm thermally grown silicon oxide. Next, Co was implanted at a fluence of 1.0×10^{17} ions/cm^2 and an energy of 80 keV. The crystallographic structure of ZnO and Co-implanted ZnO were characterized by x-ray diffraction (XRD, PANalytical X'Pert PRO MRD system). Surface characterization was performed using atomic force microscopy (AFM) in the tapping mode of operation (Dimension 3000, Veeco Instruments). The microstructure was characterized by transmission electron microscopy (TEM) on a cross section specimen cut perpendicular to the surface. The specimen was prepared using the focused ion beam (FIB) technique on a Helios NanoLab 650 machine. In order to preserve the surface layer of the sample, a carbon protective layer was deposited prior to the sample preparation. TEM investigations were performed with a FEI Tecnai G2 (200 keV, EDAX system) and a Philips CM30-FEG (300 keV, post-column GIF200 system) microscope. MR measurements were performed in a helium-4 flow cryostat with a superconducting magnet (Oxford Instruments) using an ac resistance bridge (SRS SIM921) and a four-point collinear geometry. The magnetic field H is

a)Author to whom correspondence should be addressed. Electronic mail: yujia.zeng@fys.kuleuven.be

oriented either parallel or perpendicular to the film surface, while the current is always applied perpendicular to the magnetic field for the MR measurements. The MR ratio is defined as $(R(H)\text{-}R(0))/R(0) \times 100\%$, which is smaller than the MR ratio inferred from the peak value in the hysteresis loop. The magnetization was measured with a superconducting quantum interference device (SQUID, Quantum Design MPMS XL) for fields parallel and perpendicular to the sample surface.

III. RESULTS AND DISCUSSION

In Fig. 1 we present the XRD patterns of an as-grown and a Co-implanted ZnO film. Both patterns are very similar, revealing that the Co-implanted ZnO retains its structure, even after a high-fluence implantation. The positions of the ZnO peaks and their intensity distribution indicate that the film crystallizes in the hexagonal wurtzite structure with strong (002) preferential orientation. An extra peak appears in the XRD pattern of the Co-implanted sample around $2\theta = 44°$, which can be attributed to the formation of crystalline metallic Co nanoparticles. The peak can be indexed either as the (002) peak of HCP Co or the (111) peak of FCC Co. It has been observed before that Co nanoparticles implanted in bulk ZnO single crystals crystallize into an hexagonal structure with a Co(002)||ZnO(002) preferential orientation with respect to the host matrix.[14] Presumably, a similar orientation occurs in our present study. The broadening of the Co peak is consistent with a small crystal size, which is calculated to be 6 nm using the Scherrer formula: $d = K\lambda/(\beta \cos\theta)$, where d is the average crystallite grain size, K is a numerical factor (≈ 0.9), λ is the wavelength of the x-rays, θ is the Bragg angle, and β is the full width at half maximum of the peak at 2θ in radians. However, it should be pointed out that the actual crystal size may be underestimated by the Scherrer formula due to additional broadening of the Bragg peak resulting from strain in the hybrid Co/ZnO system.

AFM measurements reveal that our ZnO films have a rather rough surface with a root-mean-square (rms) roughness around 3 nm for a surface area of $5 \times 5\ \mu m^2$. The "bombardment" effect of the high-fluence implantation slightly increases the rms roughness to around 4 nm.

The microstructure of the Co-implanted ZnO thin films is investigated by TEM. The overall composition of the film is analyzed using energy dispersive x-ray (EDX) analysis. It is found that the Co concentration (Co/[Co + Zn]) is 43 ± 5 at. %. Direct visualization of the element distribution is possible by energy filtered transmission electron microscopy (EFTEM). In Fig. 2 we present the bright field TEM image of the cross section specimen of the thin film along with the corresponding elemental maps recorded at the Zn-L, Co-L, Si-K, O-K absorption edges and a colored map composed of them. A part of the TEM sample preparation procedure was the protection of the surface by the carbon layer. Therefore the C map is shown in grey on the colored map, but not as a separate map. The Co map reveals that Co is embedded into the ZnO matrix in two different forms, i.e., evenly distributed in the ZnO matrix and in the form of Co-rich nanoprecipitates concentrated closer to the surface. The size of the precipitates in the film varies from about 5–20 nm with a mean value around 10 nm. The surface accumulation of Co nanoparticles occurs because of the combined effect of the ion implantation, which results in a Gaussian implantation profile of the Co, and the bombardment of the surface. Some of the Co nanoparticles appear in the SiO_2 substrate as well, which is unavoidable for a high-fluence implantation process. However the size of those nanoparticles which is less than 5 nm is considerably smaller than the precipitates in the film. This may influence the magnetization to a certain extent, but not significantly because the amount of Co in the substrate is small when compared to the amount of Co in the ZnO film. On the other hand, the Co in the SiO_2 should not affect the electrical transport behavior, since the implanted SiO_2 remains an insulator.

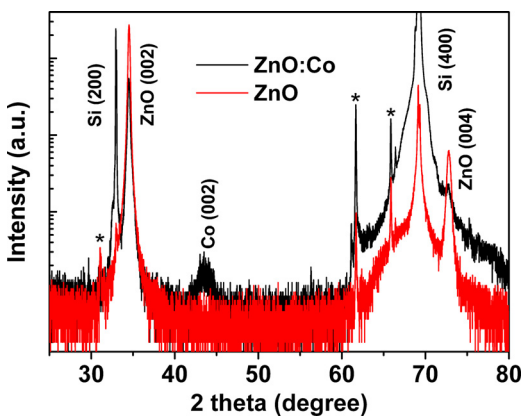

FIG. 1. XRD of a ZnO and a Co-implanted ZnO thin film on Si/SiO_2 substrates. The peaks marked with an asterisk are background peaks resulting from the strong doping of the Si.

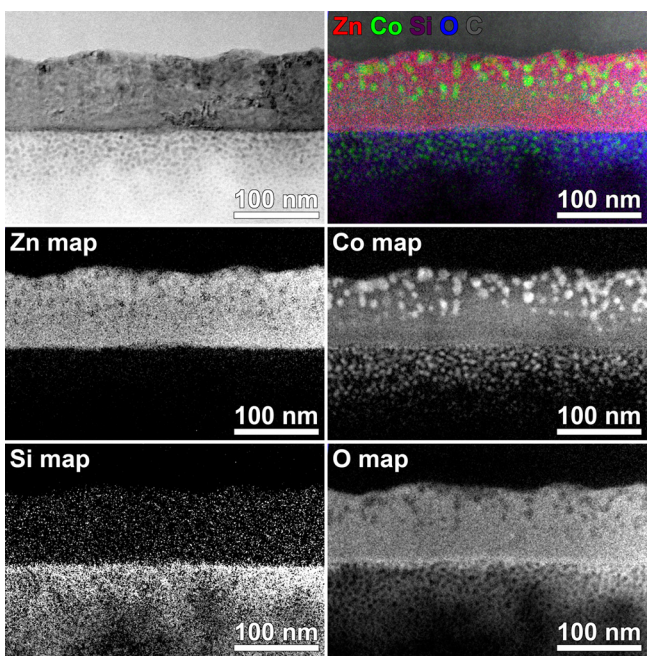

FIG. 2. Bright field TEM image of a Co-implanted ZnO thin film (upper left) and the corresponding elemental maps recorded at the Zn-L, Co-L, Si-K, O-K absorption edges and the colored map composed of them.

Comparing the elemental maps of Co and O, we find that the O map has dark spots at the position of the Co nanoparticles in the ZnO film as well as in the substrate, which indicates that in both cases the nanoparticles consist of metallic Co. The overall oxidation state of Co can be estimated using electron energy loss spectroscopy (EELS). The ratio of the L_3 and L_2 line intensities in the EELS spectra collected from the complete film (data not shown) indicates that part of the Co is oxidized. Thus, Co is present in the sample in the form of metallic Co nanoparticles and evenly distributed cobalt oxide.

The metallic Co nanoparticles are discernible on the bright field TEM images. They can be distinguished from the intrinsic features of the ZnO microstructure due to characteristic moiré fringes (see Fig. 3). The periodicity and the orientation of the fringes are defined by the mismatch between the cell parameters of the precipitates and the matrix and the mutual orientation of their lattices. The fringes of most of the particles are oriented parallel to the ZnO (001) plane, which is consistent with the results of the XRD analysis and confirms that Co nanoparticles crystallize in hexagonal structure with the preferential orientation $Co_{hcp}(002)\|ZnO(002)$.

Bright field TEM images also provide detailed information on the shape of the Co nanoparticles. Most of the particles are isolated. They have almost spherical shape, although there is a certain degree of elongation in the direction perpendicular to the surface of the film. On the other hand, relatively large particles have a complex irregular shape and seem to be composed of several crystallites. This observation is confirmed by the difference of the apparent size of the particles (5–20 nm) on the TEM images and the crystallite size estimated by the Scherrer formula (approximately 6 nm). The constituent crystallites of the large particles are slightly elongated perpendicular to the surface as well. Concerning the Co nanoparticles embedded in the substrate, the question on their crystallinity is open, since they reveal no lattice fringes on the HRTEM images and do not contribute to the electron diffraction patterns.

In Fig. 4 we plot the temperature dependence of the resistance of a Co-implanted ZnO thin film. The resistance changes slowly at high temperature but reveals typical thermally activated hopping behavior below 20 K. In our granular Co-ZnO material the conductivity is expected to be dominated by carriers that are hopping between localized impurity states when the temperature becomes sufficiently

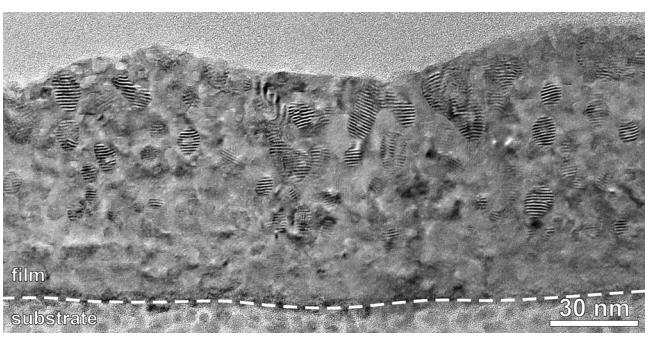

FIG. 3. Bright field TEM image of a Co-implanted ZnO thin film.

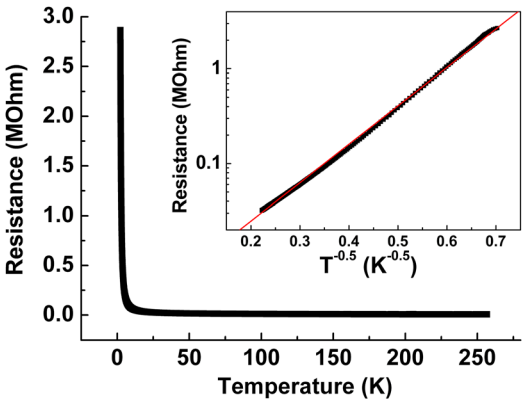

FIG. 4. Temperature dependence of the resistance of a Co-implanted ZnO thin film. The inset illustrates the fitting to the Efros-Shklovskii type VRH below 20 K.

low.[23] Mott's variable-range-hopping (VRH) predicts $R(T) \propto \exp[(T_0/T)^p]$ with $p = 1/4$ and 1/3 for a three-dimensional and a two-dimensional system, respectively.[24] On the other hand, long-range electron-electron interactions reduce the density of states at the Fermi energy, resulting in the formation of a so-called Coulomb gap. The Coulomb gap manifests itself through a modified hopping law where p increases to 1/2,[23] usually referred to as Efros-Shklovskii type VRH. The least-squares fitting of our data below 20 K (inset of Fig. 4) yields $p = 0.50 \pm 0.01$, which is consistent with the theoretical value $p = 1/2$. We conclude that the electron transport in our Co-implanted ZnO thin films becomes dominated by Efros-Shklovskii type VRH at low temperature.

Next, we turn to the spin-dependent electrical transport based on the MR and SQUID measurements, where the magnetic field is applied parallel as well as perpendicular to the sample surface for both measurements. In Figs. 5(a) and 5(b) we present the typical MR at 5 K for the Co-implanted ZnO, revealing hysteretic negative MR. On the other hand, a clear anisotropy of the MR is present, where the MR is enhanced for the perpendicular field geometry. In Fig. 5(c) we present the magnetization at 5 K for both parallel and perpendicular field. A striking feature is that the M-H curves in Fig. 5(c) exhibit a good correlation with the MR (Figs. 5(a) and 5(b)). The hysteretic MR becomes peaked at the coercive field, while the MR tends to saturate when the magnetic moment reaches saturation. The coercive field is larger when H is perpendicular to the sample surface than when H is parallel to the surface. Correspondingly, the MR peaks have a larger separation for the perpendicular geometry. The correlations between magnetism and MR point towards a pronounced spin-dependent electron transport in our Co-implanted ZnO.

We may account for the observed negative MR at low temperature in terms of a hopping version of spin-dependent scattering, which may be analogous to the well-known spin-dependent transport in granular GMR/tunnel magnetoresistance (TMR) systems. However, a detailed theoretical model of spin-dependent hopping still needs to be developed. It has been reported for $Nd_{0.52}Sr_{0.48}MnO_3$ that the resistance decrease in a magnetic field can be accounted for by a

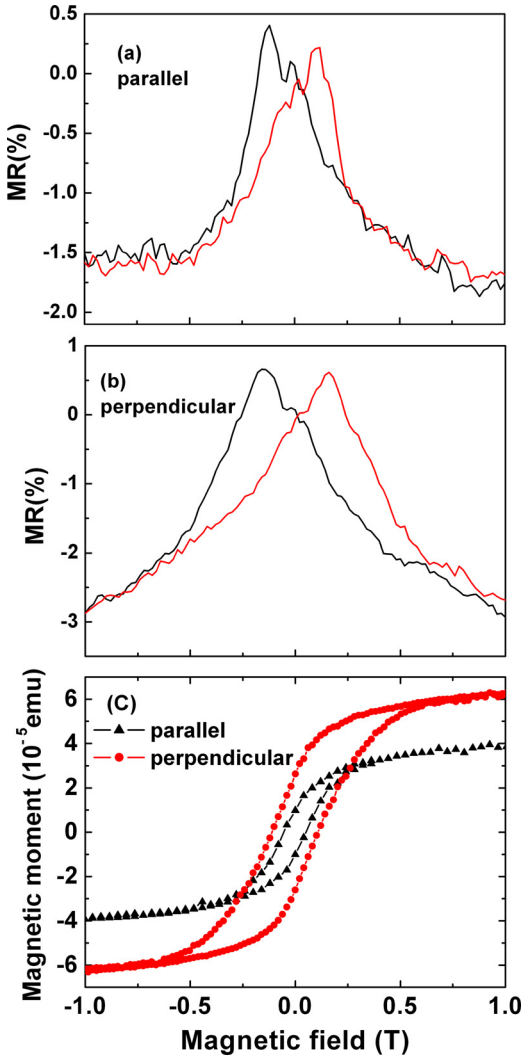

FIG. 5. Hysteretic MR loop of a Co-implanted ZnO thin film at 5 K for parallel (a) and perpendicular (b) field geometry; the red and black curves are for field forwards and backwards, respectively. (c) *M-H* curves at 5 K.

lowering of the hopping barrier due to alignment of relative magnetic moments at the hopping sites.[25] In a similar way the negative hysteretic MR in our samples may be explained in terms of a lowering of the hopping barrier between localized states that are confined to the Co nanoparticles. We note that we do not observe the hysteretic MR in samples implanted at low fluence (data not shown), in which the formation of Co nanoparticles is significantly suppressed. We therefore further confirm that the spin-dependent hopping comes from Co nanoparticles.

In Fig. 6 we present magnetization curves measured at 300 K as well as the zero-field-cooled/field-cooled (ZFC/FC) temperature dependence of the magnetization at different magnetic fields. The magnetization reveals a superparamagnetic behavior with "blocking" occurring at lower temperatures.[26] By comparing the magnetization at 300 K (Fig. 6(a)) and at 5 K (Fig. 5(c)), we find that both the coercivity and remanence decrease with increasing temperature. The disappearance of the remanent magnetization is consistent with the existence of very small, unblocked superparamagnetic Co nanoparticles at higher temperatures. In Figs. 6(b) and 6(c) the splitting between the ZFC and FC curves, which vanishes at higher temperatures, is another manifestation of the superparamagnetic behavior for both field directions. At moderate magnetic field (smaller than the saturation field), the ZFC magnetic susceptibility gradually increases (particles become unblocked) until reaching the average blocking temperature T_B, while the FC curve decreases with increasing temperature. The slow change of the curvature around T_B points towards a rather broad size distribution of the superparamagnetic clusters, which gives rise to a distribution of T_B for different cluster sizes.[26] The results for the magnetization are consistent with the results of the TEM investigations, which indicate a size of the nanoparticles varying from about 5–20 nm. One should note that the magnetization of a nanoparticle is much larger than that of the individual atoms (evenly distributed (oxidized) Co).[27,28] We therefore assume that the observed magnetic behavior is dominated by the metallic Co nanoparticles.

As indicated above, another interesting observation is the anisotropy of both the magnetization and the MR. This anisotropy may be accounted for by the fact that the easy axis of the Co nanoparticles aligns with the film normal, while the hard axis is in the film plane. This is consistent with what has been observed before in Co-implanted ZnO bulk crystals.[14] From Figs. 6(b) and 6(c) we conclude that T_B tends to shift to lower temperatures when the applied magnetic field increases. This is not unexpected since a larger magnetic field further reduces the energy barrier that blocks the fluctuation of superparamagnetic moments, allowing them to become thermally unfrozen at a lower temperature.[29–31] The above mentioned anisotropy also shows up in the shift of T_B, with a larger shift to low temperature for the parallel geometry. From Figs. 6(b) and 6(c) it becomes clear that at 0.2 T the parallel magnetization already appears to have no blocking behavior down to 5 K (no splitting of the ZFC and FC curves), while the perpendicular magnetization still reveals a blocking temperature (see arrow in Fig. 6(c)). The anisotropy can be related to the mechanisms that are discussed in more detail below and results in different energy barriers for thermal fluctuations in the parallel direction and in the perpendicular direction.

Our TEM analysis suggests a few possible mechanisms for the observed anisotropic response. First, the larger nanoparticles are mostly located quite close to the sample surface, and a considerable fraction of Co nanoparticles are elliptically shaped with their long axis along the film normal. This will induce an easy axis along the long axis due to shape anisotropy. Second, although the TEM images provide only a two-dimensional projection of the specimen, the Co nanoparticles on these images seem to be further apart in the direction parallel to the surface. This provides a possible explanation for the anisotropy in terms of the magnetic exchange interaction. The increased distance between nanoparticles in the parallel direction will result in a weakened magnetic exchange interaction, leading to a lower barrier for thermal fluctuations. Third, the anisotropy can be related to the crystal structure of the magnetic Co

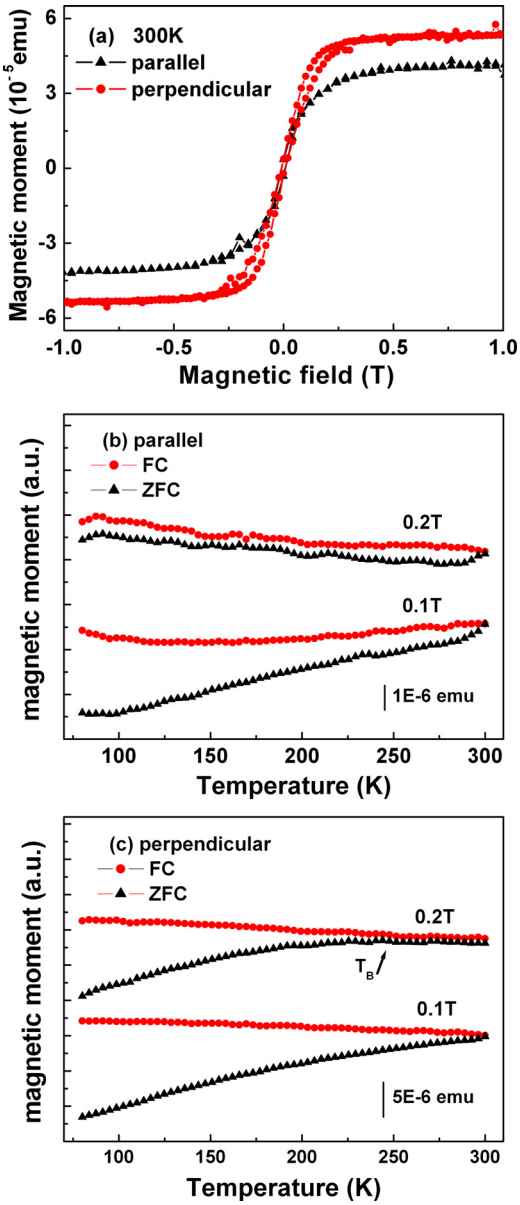

FIG. 6. (a) *M-H* curves of a Co-implanted ZnO thin film at 300 K. In (b) and (c) we present the ZFC/FC magnetization curves at different magnetic field for parallel and perpendicular field geometry, respectively. The substrate signal has been subtracted, and the curves are shifted vertically for clarity. Note that for a perpendicular field T_B is only marked for a field of 0.2 T. For 0.1 T T_B is above 300 K.

nanoparticles. From the XRD results we concluded that the Co nanoparticles appear to be crystallized along the c-axis with the same (001) preferential orientation as for the ZnO host. This will give rise to magnetocrystalline anisotropy, which originates mainly from spin-orbit (spin-lattice) interaction.[32] On the other hand, it should be pointed out that there also exist small nanoparticles whose exact shape and structure cannot be identified by XRD or TEM. Therefore, the influence of shape and magnetocrystalline anisotropy is not yet completely clear and requires further investigation. Moreover, the fact that the nanoparticles are close to the surface may also result in an additional surface induced anisotropy. Anyway, the good correlation between the SQUID and MR data confirms the existence of an anisotropic magnetic behavior, either due to one of the above mentioned anisotropies or a combination thereof. The anisotropy of the superparamagnetic system may be of technological importance for stabilizing fluctuations in applications such as magnetic recording media.

In Figs. 7(a) and 7(b) we plot the evolution of the negative MR and coercive field as a function of temperature. The negative MR ratio dramatically decreases with increasing temperature for both field directions, which is typically also observed in GMR/TMR systems. When temperature increases, more inelastic scattering processes such as electron-phonon scattering will contribute to the resistivity. This will result in a destruction of the spin-dependent transport at higher temperatures. On the other hand, the coercive field, which is inferred from the hysteretic peak positions of the MR curves, also decreases with increasing temperature, consistent with the superparamagnetism that is inferred from the SQUID data. Note that the coercivity reveals an anomalous reduction at 2.5 K. This is probably due to the fact that the ZnO matrix film itself has an intrinsic non-hysteretic MR whose contribution considerably increases at low temperature.

Although the MR ratio strongly decreases at high temperatures, the peaked MR curve survives up to 250 K, as illustrated in Figs. 8(a) and 8(b). The MR ratio is reduced to around 0.3%, but the hysteretic behavior is still clearly observed for both parallel and perpendicular geometry. The room temperature spin-dependent transport is of particular interest for magnetic sensors and spintronics. We believe there is still room for further increasing the room-temperature MR

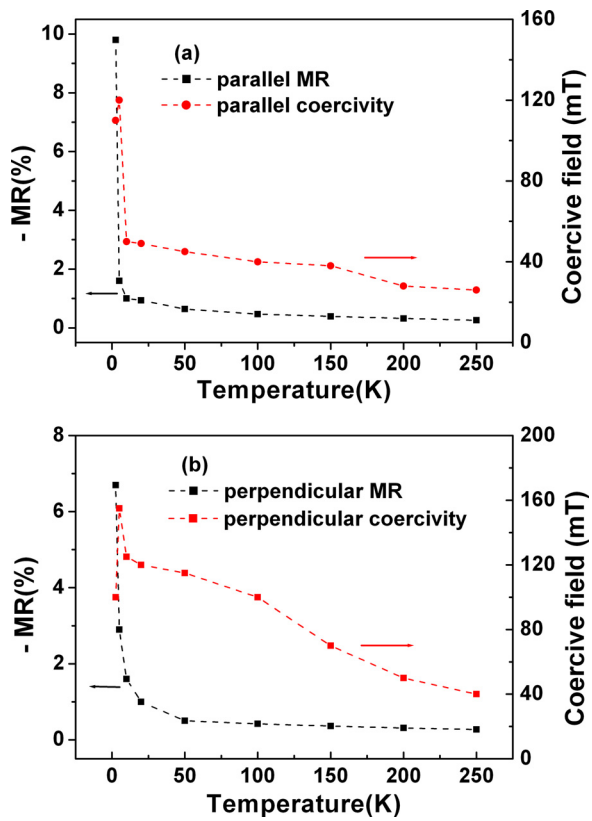

FIG. 7. MR ratio at 1 T and the coercivity inferred from the MR curves at different temperatures for parallel (a) and perpendicular (b) field geometry.

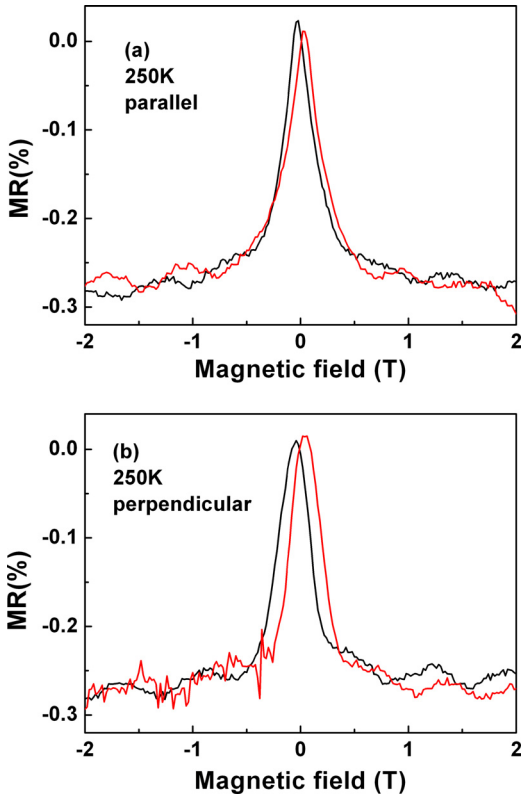

FIG. 8. Hysteretic MR loop of a Co-implanted ZnO thin film at 250 K for parallel (a) and perpendicular (b) field geometry.

ratio by suppressing the spin-independent transport mechanisms, including, in particular, the intrinsic conductivity of the ZnO host.

IV. CONCLUSIONS

In summary, we obtained oriented and elliptical Co nanoparticles embedded in ZnO thin films by combination of pulsed laser deposition of ZnO and Co ion implantation. This hybrid system displays a magnetic anisotropy, whose origin can be identified based on XRD and TEM microstructure analysis. The negative hysteretic MR is attributed to spin-dependent hopping at low temperature. In addition to the magnetization the MR also reveals anisotropy, which correlates well with the magnetization behavior. The magnetic and transport properties as well as the strong correlation between them may be used for the development of spintronic-based devices.

ACKNOWLEDGMENTS

This work was supported by the Research Foundation – Flanders (FWO, Belgium) as well as by the Belgian Interuniversity Attraction Poles (IAP P6/42) and the Flemish Concerted Research Action (GOA/09/006) research programs. D.B. would like to acknowledge Dr. Stuart Turner (EMAT, University of Antwerp) for valuable discussions and Shi Hui (EMAT, University of Antwerp) for FIB sample preparation.

[1]M. Bibes and A. Barthélémy, IEEE Trans. Electron Devices **54**, 1003 (2007).
[2]S. A. Wolf, D. D. Awschalom, R. A. Buhrman, J. M. Daughton, S. von Molnár, M. L. Roukes, A. Y. Chtchelkanova, and D. M. Treger, Science **294**, 1488 (2001).
[3]A. H. Macdonald, P. Schiffer, and N. Samarth, Nat. Mater. **4**, 195 (2005).
[4]H. Ohno, Science **281**, 951 (1998).
[5]A. E. Berkowitz, J. R. Mitchell, M. J. Carey, A. P. Young, S. Zhang, F. E. Spada, F. T. Parker, A. Hutten, and G. Thomas, Phys. Rev. Lett. **68**, 3745 (1992).
[6]J. Q. Xiao, J. S. Jiang, and C. L. Chien, Phys. Rev. Lett. **68**, 3749 (1992).
[7]A. Milner, A. Gerber, B. Groisman, M. Karpovsky, and A. Gladkikh, Phys. Rev. Lett. **76**, 475 (1996).
[8]P. C. Srivastava and J. K. Tripathi, J. Phys. D: Appl. Phys. **39**, 1465 (2006).
[9]Y. D. Park, A. Wilson, A. T. Hanbicki, J. E. Mattson, T. Ambrose, G. Spanos, and B. T. Jonker, Appl. Phys. Lett. **78**, 2739 (2001).
[10]J. W. Feng and L. P. Hwang, Appl. Phys. Lett. **75**, 1592 (1999).
[11]A. Janotti and C. G. Van de Walle, Rep. Prog. Phys. **72**, 126501 (2009).
[12]P. Stamenov, M. Venkatesan, L. S. Dorneles, D. Maude, and J. M. D. Coey, J. Appl. Phys. **99**, 08M124 (2006).
[13]S. S. Yan, C. Ren, X. Wang, Y. Xin, Z. X. Zhou, L. M. Mei, M. J. Ren, Y. X. Chen, Y. H. Liu, and H. Garmestani, Appl. Phys. Lett. **84**, 2376 (2004).
[14]S. Q. Zhou, K. Potzger, J. Von Borany, R. Grötzschel, W. Skorupa, M. Helm, and J. Fassbender, Phys. Rev. B **77**, 035209 (2008).
[15]Y. J. Zeng, L. M. C. Pereira, M. Menghini, K. Temst, A. Vantomme, J.-P. Locquet, and C. Van Haesendonck, Nano Lett. **12**, 666 (2012).
[16]N. Akdogan, H. Zabel, A. Nefedov, K. Westerholt, H. Becker, S. Gök, R. Khaibullin, and L. Tagirov, J. Appl. Phys. **105**, 043907 (2009).
[17]J. B. Cui and U. J. Gibson, Appl. Phys. Lett. **87**, 133108 (2005).
[18]F. Pan, C. Song, X. J. Liu, Y. C. Yang, and F. Zeng, Mater. Sci. Eng. R **62**, 1 (2008).
[19]J. Wang, Z. Gu, M. Lu, D. Wu, C. Yuan, S. Zhang, Y. Chen, S. Zhu, and Y. Zhu, Appl. Phys. Lett. **88**, 252110 (2006).
[20]S. Ye, V. Ney, T. Kammermeier, K. Ollefs, S. Zhou, H. Schmidt, F. Wilhelm, A. Rogalev, and A. Ney, Phys. Rev. B **80**, 245321 (2009).
[21]A. J. Behan, A. Mokhtari, H. J. Blythe, M. Ziese, A. M. Fox, and G. A. Gehring, J. Phys.: Condens. Matter **21**, 346001 (2009).
[22]N. Sharma, S. Granville, S. C. Kashyap, and J.-Ph. Ansermet, Phys. Rev. B **82**, 125211 (2010).
[23]B. I. Shklovskii and A. L. Efros, *Electronic Properties of Doped Semiconductors, Springer Series in Solid-State Sciences*, edited by M. Cardona (Springer-Verlag, 1984).
[24]N. F. Mott, J. Non-Cryst. Solids **1**, 1 (1968).
[25]P. Wagner, I. Gordon, L. Trappeniers, J. Vanacken, F. Herlach, V. V. Moshchalkov, and Y. Bruynseraede, Phys. Rev. Lett. **81**, 3980 (1998).
[26]S. Blundell, *Magnetism in Condensed Matter* (Oxford University Press, 2001).
[27]J. Jorritsma and J. A. Mydosh, IEEE Trans. Magn. **34**, 994 (1998).
[28]J. Swerts, K. Temst, C. Van Haesendonck, H. Fritzsche, V. N. Gladilin, V. M. Fomin, and J. T. Devreese, Europhys. Lett. **68**, 282 (2004).
[29]S. R. Shinde, S. B. Ogale, J. S. Higgins, H. Zheng, A. J. Millis, V. N. Kulkarni, R. Ramesh, R. L. Greene, and T. Venkatesan, Phys. Rev. Lett. **92**, 166601 (2004).
[30]J. H. Park, M. G. Kim, H. M. Jang, S. Ryu, and Y. M. Kim, Appl. Phys. Lett. **84**, 1338 (2004).
[31]S. Q. Zhou, G. Talut, K. Potzger, A. Shalimov, J. Grenzer, W. Skorupa, M. Helm, J. Fassbender, E. Čižmár, S. A. Zvyagin, and J. Wosnitza, J. Appl. Phys. **103**, 083907 (2008).
[32]B. D. Cullity and C. D. Graham, *Introduction to Magnetic Materials* (IEEE Press, Wiley, 2009).